LA-UR-17-27492 (Accepted Manuscript)

Low-Energy (<200 eV) Electron Acceleration by ULF Waves in the Plasmaspheric Boundary Layer: Van Allen Probes Observation

Funsten, Herbert O.

To be published in: Journal of Geophysical Research: Space Physics

DOI to publisher's version: 10.1002/2017JA024316

Permalink to record: http://permalink.lanl.gov/object/view?what=info:lanl-repo/lareport/LA-UR-17-27492

Low-energy (< 200 eV) electron acceleration by ULF waves in the plasmaspheric boundary layer: Van Allen Probes observation

Jie Ren,[1,2] Q. G. Zong,[1] Y. Miyoshi,[2] X. Z. Zhou,[1] Y. F. Wang,[1] R. Rankin,[3]

C. Yue,[4,5] H. E. Spence,[6] H. O. Funsten,[7] J. R. Wygant,[8] C. A. Kletzing,[9]

Q.-G.Zong, Institute of Space Physics and Applied Technologies, Peking University, Beijing 100871, China. (qgzong@pku.edu.cn)

[1]Institute of Space Physics and Applied Technology, Peking University, Beijing, China

[2]Solar-Terrestrial Environmental Laboratory, Nagoya University, Nagoya, Japan

[3]Department of Physics, University of Alberta, Edmonton, Alberta, Cananda

[4]Department of Atmospheric and Oceanic Sciences, UCLA, Los Angles, California, USA

This article has been accepted for publication and undergone full peer review but has not been through the copyediting, typesetting, pagination and proofreading process, which may lead to differences between this version and the Version of Record. Please cite this article as doi: 10.1002/2017JA024316

Abstract. We report observational evidence of cold plamsmaspheric electron (< 200 eV) acceleration by ultra-low-frequency (ULF) waves in the plasmaspheric boundary layer on 10 September 2015. Strongly enhanced cold electron fluxes in the energy spectrogram were observed along with second harmonic mode waves with a period of about 1 minute which lasted several hours during two consecutive Van Allen Probe B orbits. Cold electron (<200 eV) and energetic proton (10-20 keV) bi-directional pitch angle signatures observed during the event are suggestive of the drift-bounce resonance mechanism. The correlation between enhanced energy fluxes and ULF waves leads

[5]University Corporation for Atmospheric Research, Boulder, CO, USA

[6]Department of Physics Institute for Earth, Oceans and Space, University of New Hampshire, Durham, New Hampshire, USA

[7]Los Alamos National Laboratory,Los Alamos, USA

[8]6School of Physics and Astronomy, University of Minnesota,Twin Cities,Minneapolis,Minnesota, USA

[9]Department of Physics and Astronomy, University of Iowa, Iowa City, Iowa,, USA

to the conclusions that plasmaspheric dynamics is strongly affected by ULF waves. Van Allen Probe A and B, GOES 13, GOES 15 and MMS 1 observations suggest ULF waves in the event were strongest on the dusk-side magnetosphere. Measurements from MMS 1 contain no evidence of an external wave source during the period when ULF waves and injected energetic protons with a bump-on-tail distribution were detected by Van Allen Probe B. This suggests that the observed ULF waves were probably excited by a localized drift-bounce resonant instability, with the free energy supplied by substorm-injected energetic protons. The observations by Van Allen Probe B suggest that energy transfer between particle species in different energy ranges can take place through the action of ULF waves, demonstrating the important role of these waves in the dynamical processes of the inner magnetosphere.

1. Introduction

Ultra-low-frequency (ULF) waves in Earth's magnetosphere are geomagnetic micropulsations with mHz frequencies [*Jacobs et al.*, 1964], wavelengths comparable to the scale of the magnetosphere [*Allan and Poulter*, 1992], and largest power flux among the magnetospheric wave signals [*Lanzerotti*, 1978]. ULF waves can be excited by external (solar wind) or internal (plasma instabilities) sources. In the case of external source, there are several generating mechanisms, including the Kelvin-Helmholtz instability at the magnetopause [e.g. *Chen and Hasegawa*, 1974; *Pu and Kivelson*, 1983; *Claudepierre et al.*, 2008; *Turkakin et al.*, 2013], sudden changes in the solar wind dynamic pressure and interplanetary (IP) shock [e.g. *Zong et al.*, 2007; *Zong et al.*, 2009; *Foster et al.*, 2015], and waves in the solar wind [e.g. *Kepko et al.*, 2002; *Kepko and Spence*, 2003]. Internal sources include ion-cyclotron instability [e.g. *Yumoto et al.*, 1984; *Hughes et al.*, 1978; *Pope*, 1964], drift-bounce instability [e.g. *Southwood et al.*, 1969; *Dai et al.*, 2013], and the drift-mirror instability [e.g. *Hasegawa*, 1969; *Lanzerotti et al.*, 1969], etc.

When wave-particle interactions occur in the inner magnetosphere, the second and third adiabatic invariants can be broken when wave periods are comparable with the bounce periods of energetic ions and the drift periods of energetic electrons [*Zong et al.*, 2008]. The drift-bounce resonant condition for poloidal mode ULF waves can be described theoretically by [*Southwood et al.*, 1969] as

$$\omega - m\omega_d = N\omega_b \tag{1}$$

where ω and m are the wave angular frequency and azimuthal wave number, respectively; ω_d and ω_b are the particle drift and bounce angular frequencies, respectively; N is an integer depending on the wave harmonic modes. For odd mode (e.g. fundamental mode, third harmonic mode), N= $0, \pm 2, ...$; for even mode (e.g. second harmonic mode, fourth harmonic mode), N= $\pm 1, \pm 3, ...$ [*Southwood and Kivelson*, 1981, 1982; *Ren et al.*, 2015, 2016; *Takahashi et al.*, 1990].

An increasing number of spacecraft observations suggest ULF waves significantly affect the dynamics of charged particles in the inner magnetosphere [e.g. *Zong et al.*, 2009, 2012; *Foster et al.*, 2015; *Takahashi et al.*, 2006; *Yang et al.*, 2011a; *Ren et al.*, 2015, 2016; *Dai et al.*, 2013; *Pokhotelov et al.*, 2016; *Zhou et al.*, 2015, 2016]. In terms of particle energy and species, the inner magnetosphere can be divided into the radiation belts, ring current and plasmasphere. The outer radiation belt lies between L=3-7 and is mainly populated by electrons with energies ranging from tens of keV to several MeV. The ring current is carried by ions (H^+, O^+, etc) with tens to hundreds of keV that undergo magnetic field gradient and curvature drift around Earth [e.g. *Williams*, 1985]. The plasmasphere has a high density of trapped cold ($\sim$ eV) ions and electrons of mainly ionospheric origin [*Lemaire et al.*, 2005; *Yue et al.*, 2016]. Spacecraft observations and simulations have confirmed the important role of ULF waves in the inner magnetosphere, including their effect on radiation belt electron acceleration [*Mathie and Mann*, 2000; *Mann et al.*, 2013; *Foster et al.*, 2015], loss [*Turner et al.*, 2012; *Murphy et al.*, 2015; *Millan and Thorne*, 2007], and transport [*Pokhotelov et al.*, 2016; *Fei et al.*, 2006; *Elkington and Sarris*, 2016]. Processes associated with ring current ion wave-particle interactions have been reported, including ring current O^+ ion acceleration and deceleration [*Yang et al.*, 2011a; *Zong et al.*,

2012; *Ren et al.*, 2016], different ion species behaviors [*Ren et al.*, 2016; *Zong et al.*, 2012; *Yang et al.*, 2010], changes in pitch angle characteristics along field lines [*Yang et al.*, 2011b; *Ren et al.*, 2017], and the use of phase relationship between resonant ions and ULF waves as a diagnostic of wave electric field morphology [*Ren et al.*, 2016, 2017], etc.

The interaction between cold plasmasphere electrons and ULF waves has not been extensively investigated. *Zhang et al.* [2012] investigated the global magnetospheric response to IP shocks, and found that during the enhancement of a plasmasphere plume the ion distribution changed from isotropic to anisotropic after IP shock arrival. *Adrian et al.* [2004] studied plasmasphere features using EUV observations, and suggested that the plasmasphere configuration can change as a result of convective motion caused by standing ULF waves. *Zong et al.* [2012] reported spacecraft observation of the significant enhancement of plasmapsheric O^+ ions during the appearance of ULF waves induced by an IP shock, and suggested a possible relationship between ULF waves and the oxygen torus. *Zong et al.* [2017] found that low energy plasmaspheric electrons could be accelerated by third harmonic mode ULF waves excited by interplanetary shocks. Using Van Allen Probes observations, *Yue et al.* [2016] examined two IP shock events which showed rapid enhancement of cold (<100 eV) ion flux. Their study suggested that in addition to the $\mathbf{E} \times \mathbf{B}$ drift by the IP shock induced electric field, betatron acceleration also plays an important role in the ion flux enhancements.

In this paper, we report Van Allen Probes observations of the interaction between cold (< 200 eV) plasmapshere electrons and ULF waves when there is no IP shock impact on the magnetosphere, and study how cold electrons are accelerated by ULF waves. We also report multi-spacecraft observations of ULF waves interacting with energetic protons on a

global scale in order to explore the wave excitation mechanism. Section 2 briefly describes the methodology. Section 3 summarizes observations of ULF waves, cold electrons, and energetic protons that we analyze. Sections 4 and 5 present a discussion and conclusions of our main findings, respectively.

2. Data Set

In this paper, we mainly use Van Allen Probe B observations of electrons and protons, magnetic fields, and electric fields. The Van Allen Probes mission consists of two identically instrumented spacecraft (RBSP-A and RBSP-B), which have an orbital period of ~9 h near the equatorial plane, a perigee at ~1.1 R_E, and an apogee at ~5.8 R_E [*Mauk et al.*, 2013]. Electron and ion measurements are provided by the Helium, Oxygen, Proton and Electron (HOPE) mass spectrometer [*Funsten et al.*, 2013] and the Energetic particle, Composition, and Thermal plasma (ECT) suite [*Spence et al.*, 2013]. The spectral measurements cover an energy range from ~ 15 eV to 50 keV for electrons, and from ~ 1 eV to 50 keV for ions, including protons, He^+ and O^+. The pitch angle measurement of the HOPE instrument is divided into 11 bins. The Electric and Magnetic Field Instrument and Integrated Science (EMFISIS) instrument provides DC magnetic field measurements from DC to 30 Hz and AC electric and magnetic fields from 10 Hz up to 400 kHz [*Kletzing et al.*, 2013]. Measurements of the electric field y and z components in a Modified Geocentric Solar Ecliptic coordinate (MGSE) are obtained from the Electric Field and Waves (EFW) instrument [*Wygant et al.*, 2013]. The x component of electric field used in this study is derived by assuming $\mathbf{E} \cdot \mathbf{B} = \mathbf{0}$ when the angle between the spacecraft spin plane and magnetic field line was larger than 15° [*Dai et al.*, 2013].

On March 12, 2015, the Magnetospheric Multiscale (MMS) mission [*Burch et al.*, 2016] with four spacecraft in a tetrahedral configuration was launched into an elliptical Earth orbit with a 28.5° inclination, a perigee at 1.08 R_E, and an apogee at 12 R_E. The FluxGate Magnetometer (FGM) [*Torbert et al.*, 2016] onboard MMS 1 provides magnetic field measurements in a burst rate with a time resolution of 128 Hz. Magnetometers onboard GOES 13 and GOES 15 spacecraft provide magnetic field measurements with a time resolution of 512 ms at geosynchronous orbit.

3. Observation

3.1. Overview

Figure 1 shows the equatorial plane position in GSM coordinates for two Van Allen Probes in the inner magnetosphere, the GOES 13 and GOES 15 in geosynchronous orbit, and MMS 1 travelling inbound and outbound in the magnetosphere. From 00:00 UT to 16:00 UT on 10 September 2015, the suite of spacecraft observations cover a region of the magnetosphere with MLT ranging from 0 to 24 and L shell from 1.1 to 10, which makes it possible to explore the global distributions of ULF waves and examine possible wave sources. In-situ solar wind observations from WIND and ACE, not shown here, indicate there were low-velocity (< 450 km/s) solar wind and no sudden dynamic pressure, which implies there was no IP shock impact.

Figure 2 presents an overview of Van Allen Probe B observations with magnetic field from EMFISIS instrument, electric field from EFW instrument, and electron and proton fluxes from ECT/HOPE instrument from 20:00 UT on 9 September 2015 to 16:00 UT on 10 September 2015. The wavelet power spectra of the original B_x in Figure 2a and E_y in Figure 2c show that there exist ULF wave oscillations in the period of ~ 1 min

near the Probe B apogee during the time intervals of 01:00-04:00 UT (Part I) and 09:00-13:00 UT (Part II). During the wave appearance in wavelet power spectra, B_x and E_y component oscillations after subtracting a 10 min running average are shown in Figure 2b and 2d, respectively. The data in other times are not shown in Figure 2b and 2d because it is impossible to take away the background after subtracting a 10 min running average near the Probe B perigee. These ULF waves in the period of $\sim$ 1 min lasted several hours and are mainly distributed in the region L = 5-6. As shown in Figure 2d, there appeared ULF waves in the period of 2 min from 10:30 UT to 11:30 UT. Probe B was located near the magnetic equator where fundamental and second harmonic mode electric fields should have an anti-node and node, respectively. As shown in Figure 2d, the 2-min period ULF waves have a stronger electric field wavelet power than the 1-min period ULF waves, which indicates that 2-min and 1-min period ULF waves might be fundamental and second harmonic mode, respectively. Figure 2e - 2g show electron energy spectrum and pitch angle distributions for W>200 eV and W<200 eV, respectively. During the 1-min period ULF wave appearance, plasmasphere electrons (<200 eV) show a flux enhancement in Figure 2e and bi-directional pitch angle distributions in Figure 2g. Electrons with W> 200 eV in Figure 2f reveal a pancake-like pitch angle distribution. Figure 2h and 2k show proton energy spectrum and pitch angle distributions in different energy channels, respectively. Protons in the energy channel of 11.2 keV show a bi-directional pitch angle distribution during the 1-min period ULF wave appearance, but have a pancake-like pitch angle distribution when there are no ULF waves. Protons both in higher (e.g. 28.1 keV in Figure 2i) and lower energy channels (e.g. 2.4 keV in Figure 2k) have a pancake-like distribution during the 1-min period ULF wave appearance.

3.2. ULF Wave Properties

To explore the properties of poloidal mode ULF waves in the period of $\sim$ 1 min, magnetic and electric fields are projected into a local mean field-aligned (MFA) coordinates [*Ren et al.*, 2016; *Zong et al.*, 2012]. In Figure 3, we use magnetic and electric field data from 01:00 UT to 02:00 UT to show the phase relationship between the oscillations. Figure 3a shows B_r (radial) and E_a (azimuthal) oscillations of the poloidal mode ULF wave. E_a has a $\sim 90^\circ$ phase difference with B_r, which suggests the poloidal mode are standing waves. The wavelet power spectra of B_r in Figure 3b and E_a in Figure 3c show that the poloidal mode waves have a period of $\sim$ 1 min. The wavelet coherence analysis in Figure 3d shows the phase difference between E_a and B_r when the wavelet coherence is larger than 0.8. E_a leads B_r by 90° when Probe B is located in the northern hemisphere, which indicates the 1-min period poloidal waves are second harmonic mode ULF waves [*Singer et al.*, 1982]. The Poynting vector along the magnetic field line in Figure 3e oscillates around zero, which further indicates that the poloidal and toroidal mode field components are standing waves.

Figure 4a presents the EMFISIS spectrum of electric field spectral intensity from Probe B. The black line indicates the detected upper hybrid resonance frequency. Figure 4b shows the plasma number density derived from the upper hybrid wave dispersion relation. The plasma number density is within the range 10 to 30 cm^3 during wave appearance, which indicates that Probe B was located in the plasmasphere boundary layer. The black and red lines in Figure 4c are the calculated second harmonic mode eigenfrequency [*Degeling et al.*, 2010; *Ren et al.*, 2015] and the peak frequency from wavelet power analysis of the B_r component during wave appearance. In the modeling, we adopted an infinite

ionosphere conductance condition in both hemispheres, a power-law density variation [*Cummings et al.*, 1969] with power index of 4, and assumed the particles are all protons. The calculated wave periods are consistent with Van Allen Probe B observations in both Part I and Part II, which further indicates that the 1-min period ULF waves are second harmonic modes. The discrepancy between the modeling calculation and the observations in Part II is likely related to the assumed density distribution along the magnetic field lines.

3.3. Cold Electrons and Energetic Protons during ULF wave appearance

Figure 5a and 5b present the wavelet analysis spectra of B_r component from 00:00 UT to 06:00 UT and from 08:00 UT to 15:00 UT on 10 September 2015, respectively. In Figure 5c and 5d, electron flux with W<200 eV obviously enhanced in the parallel and anti-parallel directions during the 1-min period ULF wave appearance. For protons in Figure 5e and 5f, bi-directional pitch angle distributions appear in the energy channels from 10 keV to 20 keV during wave appearance, but pancake-like distributions are shown in the lower or higher energy channels. These observations indicate that the bi-directional pitch angle distributions for both plasmaspheric electrons (< 200 eV) and energetic protons (10-20 keV) are related to these 1-min period ULF waves. But particle flux modulations caused by ULF waves could not be observed because of the cadence (∼22 s) of HOPE instrument in comparison to ULF wave period (∼ 60 s) and some invalid data points.

Figure 6 presents the Van Allen Probe B phase space density (PSD) spectra for two orbits before ULF wave appearance (dark cyan and green), two orbits during wave appearance (red and purple), and one orbit after wave appearance (blue). The PSD spectrum for each orbit is the average PSD when Probe B was located in the region with L > 5

where ULF waves were observed by Probe B. The PSD spectra of plasmasphere electrons (<200 eV) before and after ULF wave appearance show a power-law distribution of $f = f_0 W^{-\gamma}$, where γ is the power-law index with the value of 3.5. The PSD during ULF wave appearance is enhanced up to 5 times on average. The frequency of ULF waves usually has a finite wave bandwidth, which can cause a spread in resonant energy [*Ren et al.*, 2016; *Yang et al.*, 2011a; *Takahashi et al.*, 1990]. The wave bandwidth in this study is defined by the wave power dropping from maximum to half strength [*Ren et al.*, 2016]. The gray and red shadow regions in Figure 6 indicate the resonant energy range satisfying the drift-bounce resonance with B_r wave bandwidth in Part I and Part II, respectively. We adopted the drift-bounce resonant condition with N=1 because 1-min period ULF waves are in the second harmonic mode (See details in discussion section). These HOPE observations indicate that ULF waves cause an obvious acceleration of electrons through drift-bounce resonance in the plasmasphere boundary layer.

4. Discussion

4.1. Drift-bounce Resonance of Cold Electrons and Energetic Protons

Based on Equation 1, the resonant energy of particles can be determined for a given L shell, pitch angle, and value of N when the wave frequency and azimuthal wave number are known. In Figure 7a and 7b, the resonant energy of electrons and protons versus azimuthal wave numbers is calculated to quantify the drift-bounce resonance conditions. In the calculation, the drift frequency (ω_d) includes both the magnetic field gradient-curvature drift term ($\omega_{d.gc}$) and the $\mathbf{E} \times \mathbf{B}$ drift terms due to convection ($\omega_{d.E_{con} \times B}$) and co-rotation electric fields ($\omega_{d.E_{cor} \times B}$) [*Li et al.*, 1993; *Chisham*, 1996],

$$\omega_d = -\frac{6WLP(\alpha)}{qB_E R_E^2} + \frac{2\Psi_0 L^3 sin\Phi}{B_E R_E^2} + \Omega_E \quad (2)$$

where $P(\alpha) = 0.35 + 0.15sin\alpha$ [*Hamlin et al.*, 1961], in which α is the equatorial pitch angle, W is the particle energy, L is the McIlwain L shell value, B_E is the magnetic field strength at the equator at Earth's surface, R_E is Earth's radius, Ψ_0 is the electric potential representing the dawn-dusk convection electric field, which is empirically Kp-dependent [*Maynard and Chen*, 1975], Φ is the azimuthal angle, which is positive eastward with 0° at midnight, and Ω_E is the angular frequency of Earth's rotation. For electrons of energy 1 eV to 1 keV, the drift-bounce resonant conditions N=1 and N=2 can be satisfied with $-100 < m < 100$, as shown in Figure 7a. Considering that the 1-min period ULF waves are second harmonics, only the drift-bounce resonant conditions N=1 can be satisfied, for which the resonant energy is tens of eV, which is consistent with the electron observations from the HOPE instrument in Figure 5c and 5d.

As the ULF wave frequency has a broadband bandwidth, the resonant energy should be spread over a range, as indicated by the black and red shadow regions in Figure 6. The shadow regions in Figure 6 imply that electrons of energy several eV (out of the range of measurement of the HOPE instrument) can also be influenced by ULF waves through drift-bounce resonance. For protons of energy 10 keV to 20 keV only the drift-bounce resonant condition N=1 can be satisfied, which is consistent with the proton observations from the HOPE instrument in Figure 5e and 5f. During the intervals of interest, the fluxes of >200 eV electrons and protons at 28.1 keV show some variations (decrease or increase) mainly near 90° with L shell increasing, which should result from the spatial effect and substorm activities, but have no relationship with the drift-bounce resonant

interaction with ULF waves. Because when the drift-bounce resonance is satisfied for second harmonic mode waves, the flux changes of the resonant particles should be mainly in the pitch angles near 0° and 180° [e.g. *Yang et al.*, 2011b; *Ren et al.*, 2017]. We further checked other wave activities, such as EMIC and VLF waves, and their possible effect on the cold electron acceleration and bi-directional pitch angle distributions. Some chorus waves in the frequency range of 0.1-0.5 f_{ce} appeared during Part I and two previous orbits, but there was no cold electron acceleration during two previous orbits. There were almost no EMIC wave observations during Part I, Part II, and two former orbits. All there observations indicate that the cold electron acceleration and bi-directional pitch angle distributions during Part I and Part II have no apparent relationship with VLF and EMIC wave activities.

Figure 7c gives a schematic to explain the electron acceleration by second harmonic mode electric fields in the drift-bounce resonant condition N=1. When the drift-bounce resonant electrons with a certain equatorial pitch angle have a mirror point at the anti-nodes of wave electric fields in both hemispheres, they will experience the largest accelerating electric fields and get the largest net acceleration in one bounce period. Assuming that the anti-nodes are located in Mlat= ±45°, the equatorial pitch angle for electrons with maximum acceleration is about 16° according to $sin^2\alpha_{eq} = \frac{cos^6\lambda_m}{(1+3sin^2\lambda_m)^{(1/2)}}$, where α_{eq} is the equatorial pitch angle, and λ_m is the magnetic latitude of mirror point. This value is within the second and penultimate pitch angle bins of the HOPE instruments. When the equatorial pitch angle is closer to the perpendicular direction, the net acceleration in one bounce period will be weaker. This explains why the drift-bounce resonant elec-

trons (Figure 5c and 5d) and protons (Figure 5d and 5f) show bi-directional pitch angle distributions.

The PSD spectra in Figure 6 indicate that cold electrons were accelerated when there were 1-min period ULF waves. Based on the drift-bounce resonance theory, the resonant electrons will get a net energy from waves and their PSD will increase when more particles are transported into accelerating regions with westward E_a than those into decelerating regions with eastward E_a [*McPherron*, 2005; *Dai et al.*, 2013; *Ren et al.*, 2016]. The plasmasphere electron energy change can be written as

$$\frac{dW}{dt} = q\mathbf{V_d} \cdot \mathbf{E} \tag{3}$$

where $\mathbf{V_d} = \mathbf{V_{d.gc}} + \mathbf{V_{d.E\times B}} + \mathbf{V_{d.p}}$, in which $\mathbf{V_{d.gc}}$, $\mathbf{V_{d.E\times B}}$, and $\mathbf{V_{d.p}}$ are drift velocity from magnetic field gradient-curvature drift, $\mathbf{E} \times \mathbf{B}$ drift and polarization drift, respectively; $\mathbf{E} = \mathbf{E_w} + \mathbf{E_{con.}} + \mathbf{E_{cor.}}$, in which $\mathbf{E_w}$, $\mathbf{E_{con.}}$, and $\mathbf{E_{cor.}}$ are wave, convection and corotation electric fields, respectively. Wave electric field ($\mathbf{E_w}$) consists of azimuthal component ($\mathbf{E_a}$) and radial component ($\mathbf{E_r}$). Adopting $Kp = 3$, $\Phi = 50°$, $\gamma = 2$, and $L = 5.5$, the convection electric field ($\mathbf{E_{con.}}$) in the azimuthal direction is about 0.15 mV/m. In Part I and Part II, the electric field data in the time range from 01:00 UT to 03:30 UT can be projected into MFA coordinate system to obtain E_a component, which meet the requirement that the angle between the spacecraft spin and magnetic field line is larger than 15° [*Dai et al.*, 2013]. The amplitude of $\mathbf{E_a}$ in this time range is mainly from 0.5 mV/m to 1 mV/m, which is the value of second harmonic mode near the magnetic equator. The amplitude should be larger when the magnetic latitude is approaching the anti-node of the second harmonic mode electric field [e.g. *Cummings et al.*, 1969; *Takahashi et al.*, 2011], so

$\mathbf{E_a} \gg \mathbf{E_{con.}}$. For 10 eV electrons at L=5.5, $\omega_{d.gc} \sim 10^{-4}$ mHz $\cdot$ rad and $\omega_{d.p} \sim 10^{-6}$ mHz $\cdot$ rad. So $\mathbf{V_{d.gc}} \gg \mathbf{V_{d.p}}$. Considering $(\mathbf{E} \times \mathbf{B}) \cdot \mathbf{E} = \mathbf{0}$, $\mathbf{V_{d.gc}} \gg \mathbf{V_{d.p}}$, and $\mathbf{E_a} \gg \mathbf{E_{con.}}$, then Equation 3 can be rewritten as

$$\frac{dW}{dt} \simeq sqV_{d.gc}E_a \tag{4}$$

where $s = 1$ when $\mathbf{E_a} < \mathbf{0}$ (westward), and $s = -1$ when $\mathbf{E_a} > \mathbf{0}$ (eastward). Equation 4 indicates that plasmasphere electron energy change is mainly from magnetic field gradient-curvature drift and poloidal mode electric field. The PSD change caused by energy change can be expressed as $\delta f|_W = -\delta W \frac{\partial f}{\partial W}$. Then the relative PSD change can be written as $\frac{\delta f}{f}|_W = \gamma \frac{\delta W}{W}$. By taking $\delta W = sqV_{d.gc}\delta E_a$, $V_{d.gc} = -\frac{6WL^2P(\alpha)}{qB_E^2R_E}$, and $f = f_0W^{-\gamma}$, we can get $\frac{\delta f}{f}|_W = -\frac{6\gamma sL^2P(\alpha)\delta E_a}{B_E^2R_E}$, in which the relative PSD change is related to power index (γ) but not particle energy (W) and particle species [*Ren et al.*, 2016]. Therefore, cold electrons experience acceleration by ULF waves similar to energetic oxygen and proton acceleration. In reality, the PSD variation depends not only on energy change ($\frac{\delta f}{f}|_E$), but also on the radial displacement ($\frac{\delta f}{f}|_L$), because $\delta f = -\delta W \frac{\partial f}{\partial W} - \delta L \frac{\partial f}{\partial L}$ [*Southwood and Kivelson*, 1981]. In other words, the PSD variation is not only related to how much wave energy is transformed to particle energy, but also on how many particles are transported into the accelerating and decelerating regions, respectively [*McPherron*, 2005; *Dai et al.*, 2013; *Ren et al.*, 2016].

4.2. Possible Excitation Mechanism of ULF Waves

In Figure 1, multi-spacecraft observations in different regions of magnetosphere provide a good chance to explore the global distributions of ULF waves and their excitation

mechanism. Figure 8 shows the wavelet power analyses of original B_x component and its oscillations after subtracting a 10 min running average from Probe A (Figure 8a), MMS 1 (Figure 8b), GOES 13 (Figure 8c) and GOES 15 (Figure 8d). The Mlat is labelled at the bottom. From 00:00 UT to 16:00 UT on 10 September 2015, the MLTs of the 1-min period ULF wave appearance are listed in Table 1. Their values are within the range from 12 to 24 MLT, which indicates these ULF waves were distributed in the duskside. Among all the spacecraft in this study, only MMS could travel inbound and outbound in the magnetosphere to verify whether there were external sources for ULF waves or not. From the wavelet power analysis in Figure 8b, it could be found that the periods of ULF waves increased with increasing L values during the inbound and outbound passing of MMS 1, and the wave power was discountinuous in the outer region, which indicates these waves were not from external sources. At the end of 9 September 2015, there occurred two large substorms with AL index up to -1000 nT, and substorm injections were observed by GOES spacecraft (not shown here). From observations of Probe B, the energetic protons with bump-on-tail plasma distributions at $\sim$ 10 keV (not shown here) interacted with 1-min ULF waves through drift-bounce resonance.

All the aforementioned observations imply that these waves were generated through drift-bounce instability with the free energy from a bump-on-tail distribution of substorm-injected protons [e.g. *Liu et al.*, 2013]. From the magnetic field observations of MMS 1, the continuous variations of the wave period with increasing L shell values range from Pc3 (10-45 s) to Pc4 (45-150 s), which indicates the wave period is controlled by the resonance properties (e.g. eigenfrequency) of the magnetic field lines [*Surkov and Hayakawa*, 2014]. Previous studies found that there were two main sources of Pc3 including upstream waves

related to the ion cyclotron instability in the Earth's foreshock [e.g. *Miura*, 1984; *Eastwood et al.*, 2005, 2011] and surface waves excited by Kelvin-Helmhotz instability [e.g. *Southwood*, 1979; *Miura*, 1984]. This study suggests that ULF waves in the period of Pc 3 also can be generated through drift-bounce instability when substorm particles are injected into enough deeper regions in the inner magnetosphere.

5. Conclusion

The objective of this paper is to explore the role of ULF waves in the dynamics of cold plasmasphere electrons with Van Allen Probes observation. The main findings are summarized as follows.

1. When Van Allen Probe B was travelling through the plasmasphere boundary layer on September 10th, 2015, long-lasting (several hours) ULF waves with a period on the order of $\sim$ 1 minute were observed over two consecutive orbits. These ULF waves are identified as second harmonic modes because (1) their electric field intensity is lower than that of 2 minute period ULF waves near the magnetic equator and their magnetic field power is higher; (2) E_a leads B_r by 90° at magnetic latitudes larger than 0°; (3) the observed wave period is consistent with the estimated second harmonic mode eigenperiod; (4) they satisfy the drift-bounce resonance condition with N= 1 for both cold electrons and energetic protons.

2. A bi-directional pitch angle distribution was observed for both cold electrons (<200 eV) and energetic protons (10-20 keV) when the 1 minute period ULF waves appeared, which is expected from drift-bounce resonance with ULF waves. From the electron PSD spectra in five orbits, it was found that cold electron fluxes during the interval when ULF waves appeared were enhanced by up to several times the background power-law

distribution when no ULF waves are present, which demonstrates the important role of ULF waves in the dynamics of cold electrons in the inner magnetosphere.

3. According to global observations from both Van Allen Probes, GOES 13 and GOES 15, and MMS 1, it is found that the 1 minute period ULF waves are mainly confined to the dusk side. No external sources were observed by MMS 1 when it was travelling inbound and outbound in the outer magnetosphere. During the same interval, Van Allen Probe B observed drift-bounce resonance between 1 minute period ULF waves and substorm-injected energetic protons in a bump-on-tail distribution. All these phenomena indicate that the 1 minute period ULF waves were excited through the drift-bounce resonance instability and that cold plasmaspheric electrons and substorm-injected energetic protons are connected through the energy transferred to them by ULF waves.

This study presented in this paper shows that cold (∼15-200 eV) electrons interact efficiently with 1 minute period ULF waves. The evidence suggests that even colder electrons ($\sim$ eV) will be affected by ULF waves, although this possibility cannot be confirmed by the Van Allen Probes as because the energies are out of the range of measurement. Based on the drift-bounce resonance condition, cold electrons can be affected by ULF waves at even lower frequencies (e.g. Pc5). Even though plasmasphere electrons of energy $\sim$ 1 eV are invisible to instruments, their interaction with ULF waves can be inferred from the behaviour of higher-energy electrons that satisfy the drift-bounce resonance condition for broadband ULF waves. More event studies and statistical studies are needed to improve understanding of the role of ULF waves in the dynamics of the plasmasphere.

Acknowledgments. This work was supported by the National Natural Science Foundation of China (41627805) and Major Project of Chinese National Programs for Fun-

damental Research and Development (2012CB825603). R. Rankin acknowledges the financial support of NSERC and the Canadian Space Agency. Chao Yue gratefully acknowledges support from NASA Living With a Star Jack Eddy Postdoctoral Fellowship Program, administered by the UCAR Visiting Scientist Programs. We acknowledge use of Van Allen Probes data (ftp://cdaweb.gsfc.nasa.gov/pub/data/rbsp/), MMS data (https://lasp.colorado.edu/mms/sdc/public/), and GOES data (https://satdat.ngdc.noaa.gov/sem/goe

References

Adrian, M., D. Gallagher, and L. Avanov, Image euv observation of radially bifurcated plasmaspheric features: First observations of a possible standing ULF waveform in the inner magnetosphere, *J. Geophys. Res.*, *109*(A1), doi:10.1029/2003JA009974, 2004.

Allan, W., and E. Poulter, ULF waves-their relationship to the structure of the earth's magnetosphere, *Reports on Progress in Physics*, *55*(5), 533, 1992.

Burch, J. L., T. E. Moore, R. B. Torbert, and B. L. Giles, Magnetospheric multiscale overview and science objectives, *Space Sci. Rev.*, *199*(1-4), 5–21, doi:10.1007/s11,214–015–0164–9, 2016.

Chen, L., and A. Hasegawa, A theory of long-period magnetic pulsations: 2. impulse excitation of surface eigenmode, *J. Geophys. Res.*, *79*(7), 1033–1037, doi:10.1029/JA079i007p01033, 1974.

Chisham, G., Giant pulsations: An explanation for their rarity and, *J. Geophys. Res.*, *101*(A11), 24–755, doi:10.1029/96JA02540, 1996.

Claudepierre, S., S. Elkington, and M. Wiltberger, Solar wind driving of magnetospheric ULF waves: Pulsations driven by velocity shear at the magnetopause, *J. Geophys. Res.*,

113(A5), doi:10.1029/2007JA012890, 2008.

Cummings, W., R. O'sullivan, and P. Coleman, Standing alfvén waves in the magnetosphere, *J. Geophys. Res.*, *74*(3), 778–793, doi:10.1029/JA074i003p00778, 1969.

Dai, L., et al., Excitation of poloidal standing alfvén waves through drift resonance wave-particle interaction, *Geophys. Res. Lett.*, *40*(16), 4127–4132, doi:10.1002/grl.50800, 2013.

Degeling, A., R. Rankin, K. Kabin, I. Rae, and F. Fenrich, Modeling ULF waves in a compressed dipole magnetic field, *J. Geophys. Res.*, *115*(A10), 2010.

Eastwood, J., A. Balogh, E. Lucek, C. Mazelle, and I. Dandouras, Quasi-monochromatic ULF foreshock waves as observed by the four-spacecraft cluster mission: 1. statistical properties, *J. Geophys. Res.*, *110*(A11), doi:10.1029/2004JA010617, 2005.

Eastwood, J., S. Schwartz, T. Horbury, C. Carr, K.-H. Glassmeier, I. Richter, C. Koenders, F. Plaschke, and J. Wild, Transient pc3 wave activity generated by a hot flow anomaly: Cluster, rosetta, and ground-based observations, *J. Geophys. Res.*, *116*(A8), doi:10.1029/2011JA016467, 2011.

Elkington, S. R., and T. E. Sarris, The role of Pc-5 ULF waves in the radiation belts: Current understanding and open questions, *Waves, Particles, and Storms in Geospace: A Complex Interplay*, p. 80, 2016.

Fei, Y., A. A. Chan, S. R. Elkington, and M. J. Wiltberger, Radial diffusion and mhd particle simulations of relativistic electron transport by ULF waves in the september 1998 storm, *J. Geophys. Res.*, *111*(A12), doi:10.1029/2005JA011211, 2006.

Foster, J., J. Wygant, M. Hudson, A. Boyd, D. Baker, P. Erickson, and H. E. Spence, Shock-induced prompt relativistic electron acceleration in the inner magnetosphere, *J.*

Geophys. Res., *120*(3), 1661–1674, doi:10.1002/2014JA020642, 2015.

Funsten, H., et al., Helium, oxygen, proton, and electron (hope) mass spectrometer for the radiation belt storm probes mission, *Space Sci. Rev.*, *179*(1-4), 423–484, doi:10.1007/s11,214–013–9968–7, 2013.

Hamlin, D. A., R. Karplus, R. C. Vik, and K. M. Watson, Mirror and azimuthal drift frequencies for geomagnetically trapped particles, *J. Geophys. Res.*, *66(1)*, 1C4, doi:10.1029/JZ066i001p00,001, 1961.

Hasegawa, A., Drift mirror instability in the magnetosphere, *The Physics of Fluids*, *12*(12), 2642–2650, 1969.

Hughes, W., D. Southwood, B. Mauk, R. McPherron, and J. Barfield, Alfvén waves generated by an inverted plasma energy distribution, *Nature*, *275*(5675), 43–45, doi:10.1038/275043a0, 1978.

Jacobs, J., Y. Kato, S. Matsushita, and V. Troitskaya, Classification of geomagnetic micropulsations, *J. Geophys. Res.*, *69*(1), 180–181, 1964.

Kepko, L., and H. E. Spence, Observations of discrete, global magnetospheric oscillations directly driven by solar wind density variations, *J. Geophys. Res.*, *108*(A6), doi:10.1029/2002JA009676, 2003.

Kepko, L., H. E. Spence, and H. Singer, ULF waves in the solar wind as direct drivers of magnetospheric pulsations, *Geophys. Res. Lett.*, *29*(8), doi:10.1029/2001GL014405, 2002.

Kletzing, C., et al., The electric and magnetic field instrument suite and integrated science (emfisis) on rbsp, *Space Sci. Rev.*, *179*, 127–181, doi:10.1007/s11,214–013–9993–6, 2013.

Lanzerotti, L., Studies of geomagnetic pulsations, *Upper Atmosphere Research in Antarctica*, pp. 130–156, doi:10.1029/AR029p0130, 1978.

Lanzerotti, L., A. Hasegawa, and C. Maclennan, Drift mirror instability in the magnetosphere: Particle and field oscillations and electron heating, *J. Geophys. Res.*, *74*(24), 5565–5578, doi:10.1029/JA074i024p05565, 1969.

Lemaire, J. F., K. I. Gringauz, D. L. Carpenter, and V. Bassolo, The earth's plasmasphere, Cambridge University Press, 2005.

Li, X., M. Hudson, A. Chan, and I. Roth, Loss of ring current o+ ions due to interaction with pc 5 waves, *J. Geophys. Res.*, *98*(A1), 215–231, doi:10.1029/92JA01540, 1993.

Liu, W., et al., Poloidal ULF wave observed in the plasmasphere boundary layer, *J. Geophys. Res.*, *118*(7), 4298–4307, doi:10.1002/jgra.50427, 2013.

Mann, I. R., et al., Discovery of the action of a geophysical synchrotron in the earths van allen radiation belts, *Nature communications*, *4*, doi:doi:10.1038/ncomms3795, 2013.

Mathie, R., and I. Mann, A correlation between extended intervals of ULF wave power and storm-time geosynchronous relativistic electron flux enhancements, *Geophys. Res. Lett.*, *27*(20), 3261–3264, doi:10.1029/2000GL003822, 2000.

Mauk, B., N. J. Fox, S. Kanekal, R. Kessel, D. Sibeck, and A. Ukhorskiy, Science objectives and rationale for the radiation belt storm probes mission, *Space Sci. Rev.*, *179*(1-4), 3–27, doi:10.1007/s11,214–012–9908–y, 2013.

Maynard, N., and A. Chen, Isolated cold plasma regions: Observations and their relation to possible production mechanisms, *J. Geophys. Res.*, *80*(7), 1009–1013, doi:10.1029/JA080i007p01009, 1975.

McPherron, R. L., Magnetic pulsations: their sources and relation to solar wind and geomagnetic activity, *Surveys in Geophysics*, *26*(5), 545–592, doi:10.1007/s10,712–005–1758–7, 2005.

Millan, R., and R. Thorne, Review of radiation belt relativistic electron losses, *Journal of Atmospheric and Solar-Terrestrial Physics*, *69*(3), 362–377, 2007.

Miura, A., Anomalous transport by magnetohydrodynamic kelvin-helmholtz instabilities in the solar wind-magnetosphere interaction, *J. Geophys. Res.*, *89*(A2), 801–818, doi:10.1029/JA089iA02p00801, 1984.

Murphy, K. R., I. R. Mann, and D. G. Sibeck, On the dependence of storm time ULF wave power on magnetopause location: Impacts for ULF wave radial diffusion, *Geophys. Res. Lett.*, *42*(22), 9676–9684, doi:10.1002/2015GL066592, 2015.

Pokhotelov, D., I. Rae, K. Murphy, and I. Mann, Effects of ULF wave power on relativistic radiation belt electrons: 8–9 october 2012 geomagnetic storm, *J. Geophys. Res.*, *121*, 11,766–11,779, doi:10.1002/2016JA023130, 2016.

Pope, J. H., An explanation for the apparent polarization of some geomagnetic micropulsations (pearls), *J. Geophys. Res.*, *69*(3), 399–405, doi:10.1029/JZ069i003p00399, 1964.

Pu, Z.-Y., and M. G. Kivelson, Kelvin: Helmholtz instability at the magnetopause: Solution for compressible plasmas, *J. Geophys. Res.*, *88*(A2), 841–852, doi:10.1029/JA088iA02p00841, 1983.

Ren, J., Q. G. Zong, Y. F. Wang, and X. Z. Zhou, The interaction between ULF waves and thermal plasma ions at the plasmaspheric boundary layer during substorm activity, *J. Geophys. Res.*, *120*(2), 1133–1143, doi:10.1002/2014JA020766, 2015.

Ren, J., Q. G. Zong, X. Z. Zhou, R. Rankin, and Y. F. Wang, Interaction of ULF waves with different ion species: pitch angle and phase space density implications, *J. Geophys. Res.*, *121*(10), 9459–9472, doi:10.1002/2016JA022995, 2016.

Ren, J., Q. G. Zong, X. Z. Zhou, R. Rankin, Y. F. Wang, S. J. Gu, and Y. F. Zhu, Phase relationship between ULF waves and drift-bounce resonant ions: a statistical study, *J. Geophys. Res.*, doi:10.1002/2016JA023848, 2017.

Singer, H. J., W. J. Hughes, and C. T. Russell, Standing Hydromagnetic Waves Observed by ISEE 1 and 2: Radial Extent and Harmonic, *J. Geophys. Res.*, *87*, 3519–3529, doi:10.1029/JA087iA05p03519, 1982.

Southwood, D., Magnetopause kelvin-helmholtz instability, in *Magnetospheric Boundary Layers*, vol. 148, pp. 357–364, 1979.

Southwood, D., J. Dungey, and R. Etherington, Bounce resonant interaction between pulsations and trapped particles, *Planet. Space Sci.*, *17*(3), 349–361, 1969.

Southwood, D. J., and M. G. Kivelson, Charged particle behavior in low-frequency geomagnetic pulsations. i transverse waves, *J. Geophys. Res.*, *86*, 5643–5655, doi:10.1029/JA086iA07p05643, 1981.

Southwood, D. J., and M. G. Kivelson, Charged particle behavior in low-frequency geomagnetic pulsations. ii - graphical approach, *J. Geophys. Res.*, *87*, 1707–1710, 1982.

Spence, H. E., et al., Science goals and overview of the radiation belt storm probes (rbsp) energetic particle, composition, and thermal plasma (ect) suite on nasas van allen probes mission, *Space Sci. Rev.*, *179*(1-4), 311–336, doi:10.1007/s11214-013-0007-5, 2013.

Surkov, V., and M. Hayakawa, Ultra and extremely low frequency electromagnetic fields, Springer, 2014.

Takahashi, K., R. McEntire, A. Lui, and T. Potemra, Ion flux oscillations associated with a radially polarized transverse pc 5 magnetic pulsation, *J. Geophys. Res.*, *95*(A4), 3717–3731, doi:10.1029/JA095iA04p03717, 1990.

Takahashi, K., P. J. Chi, R. E. Denton, and R. L. Lysak, Magnetospheric ULF waves: Synthesis and new directions. geophysical monograph 169, in *Magnetospheric ULF Waves: Synthesis and New Directions*, vol. 169, 2006.

Takahashi, K., K.-H. Glassmeier, V. Angelopoulos, J. Bonnell, Y. Nishimura, H. J. Singer, and C. T. Russell, Multisatellite observations of a giant pulsation event, *J. Geophys. Res.*, *116*(A11), doi:10.1029/2011JA016955, 2011.

Torbert, R., et al., The fields instrument suite on mms: scientific objectives, measurements, and data products, *Space Sci. Rev.*, *199*(1-4), 105–135, doi:10.1007/s11214-014-0109-8, 2016.

Turkakin, H., R. Rankin, and I. Mann, Primary and secondary compressible kelvin-helmholtz surface wave instabilities on the earth's magnetopause, *J. Geophys. Res.*, *118*(7), 4161–4175, doi:10.1002/jgra.50394, 2013.

Turner, D. L., Y. Shprits, M. Hartinger, and V. Angelopoulos, Explaining sudden losses of outer radiation belt electrons during geomagnetic storms, *Nature Physics*, *8*(3), 208–212, doi:doi:10.1038/nphys2185, 2012.

Williams, D., Dynamics of the earth's ring current: Theory and observation, *Space Sci. Rev.*, *42*(3-4), 375–396, doi:doi:10.1007/BF00214994, 1985.

Wygant, J., et al., The electric field and waves instruments on the radiation belt storm probes mission, *Space Sci. Rev.*, *179*(1-4), 183–220, doi:10.1007/s11214-013-0013-7, 2013.

Yang, B., Q.-G. Zong, Y. Wang, S. Fu, P. Song, H. Fu, A. Korth, T. Tian, and H. Reme, Cluster observations of simultaneous resonant interactions of ULF waves with energetic electrons and thermal ion species in the inner magnetosphere, *J. Geophys. Res.*, *115*(A2), doi:10.1029/2009JA014542, 2010.

Yang, B., Q.-G. Zong, S. Y. Fu, X. Li, A. Korth, H. S. Fu, C. Yue, and H. Reme, The role of ULF waves interacting with oxygen ions at the outer ring current during storm times, *J. Geophys. Res.*, *116*, doi:10.1029/2010JA015683, 2011a.

Yang, B., et al., Pitch angle evolutions of oxygen ions driven by storm time ULF poloidal standing waves, *J. Geophys. Res.*, *116*, doi:A03207, doi:10.1029/2010JA016047, 2011b.

Yue, C., et al., Rapid enhancement of low-energy (¡ 100 ev) ion flux in response to interplanetary shocks based on two van allen probes case studies: Implications for source regions and heating mechanisms, *J. Geophys. Res.*, *121*(7), 6430–6443, doi:10.1002/2016JA022808, 2016.

Yumoto, K., T. Saito, B. T. Tsurutani, E. J. Smith, and S.-I. Akasofu, Relationship between the imf magnitude and pc 3 magnetic pulsations in the magnetosphere, *J. Geophys. Res.*, *89*(A11), 9731–9740, doi:10.1029/JA089iA11p09731, 1984.

Zhang, H., D. G. Sibeck, Q.-G. Zong, J. P. McFadden, D. Larson, K.-H. Glassmeier, and V. Angelopoulos, Global magnetospheric response to an interplanetary shock: Themis observations, *30*(2), 379, 2012.

Zhou, X.-Z., Z.-H. Wang, Q.-G. Zong, R. Rankin, M. G. Kivelson, X.-R. Chen, J. B. Blake, J. R. Wygant, and C. A. Kletzing, Charged particle behavior in the growth and damping stages of ultralow frequency waves: theory and van allen probes observations, *J. Geophys. Res.*, doi:10.1002/2016JA022447, 2016.

Zhou, X.-Z., et al., Imprints of impulse-excited hydromagnetic waves on electrons in the van allen radiation belts, *Geophys. Res. Lett.*, *42*(15), 6199–6204, doi: 10.1002/2015GL064988, 2015.

Zong, Q.-G., Y. F. Wang, B. Yang, S. Y. Fu, Z. Y. Pu, L. Xie, and T. A. Fritz, Recent progress on ULF wave and its interactions with energetic particles in the inner magnetosphere, *Science in China Series E: Technological Sciences*, *51*(10), 1620–1625, doi:10.1007/s11431-008-0253-z, 2008.

Zong, Q.-G., Y. F. Wang, H. Zhang, S. Y. Fu, H. Zhang, C. R. Wang, C. J. Yuan, and I. Vogiatzis, Fast acceleration of inner magnetospheric hydrogen and oxygen ions by shock induced ULF waves, *J. Geophys. Res.*, *117*, A11,206, doi:10.1029/2012JA018,024, 2012.

Zong, Q.-G., et al., Ultralow frequency modulation of energetic particles in the dayside magnetosphere, *Geophys. Res. Lett.*, *34*, 12,105–+, doi:10.1029/2007GL029915, 2007.

Zong, Q.-G., et al., Energetic electrons response to ULF waves induced by interplanetary shocks in the outer radiation belt, *J. Geophys. Res.*, *114*, A10,204, doi:10.1029/2009JA014,393, 2009.

Zong, Q.-G., Y. F. Wang, J. Ren, X. Z. Zhou, S. Y. Fu, R. Rankin, and H. Zhang, Corotating drift-bounce resonance of plasmaspheric electron with poloidal ULF waves, *Earth and Planetary Physics*, *1*, doi:10.26464/epp2017002, 2017.

Table 1. MLTs of different spacecraft observing the 1-min period ULF waves from 00:00 UT to 16:00 UT on 10 September 2015

Satellite	RBSP-B	RBSP-A	MMS 1	GOES 13	GOES15
MLT	14.3-16.8 13.8-16.8	14.8-16.5 13.6-15.0	19.6-20.3 13.7-14.7	20.0-24.0	18.0-23.0

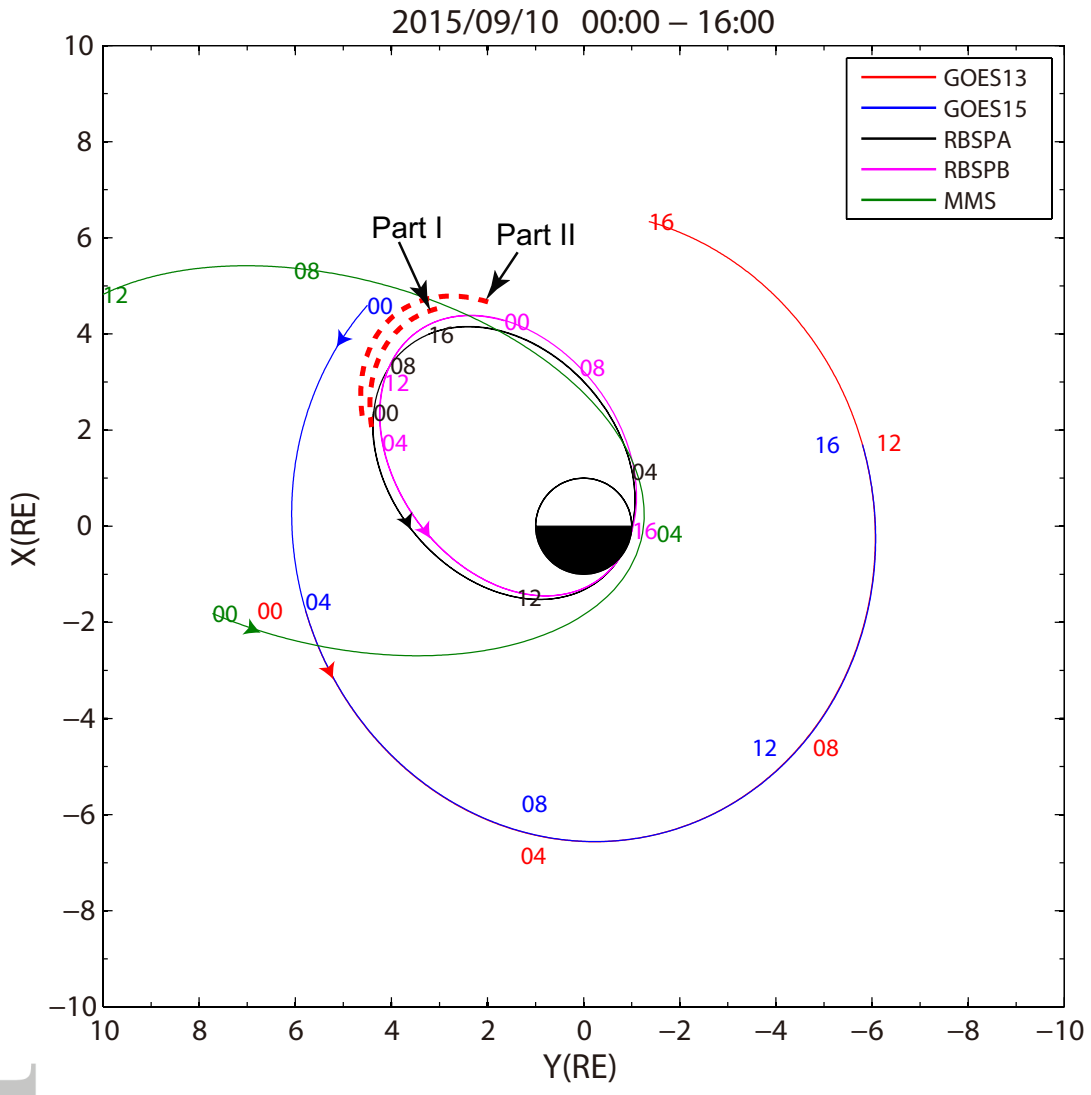

Figure 1. Equatorial plane positions in GSM coordinates for two Van Allen Probes in the inner magnetosphere, two GOES spacecraft (GOES 13 and GOES 15) in the geosynchronous orbit, and MMS 1 travelling inbound and outbound in the magnetosphere. The red dashed lines represent the time intervals of interest (Part I: 01:00-04:00 UT and Part II: 09:00-13:00 UT) in Probe B.

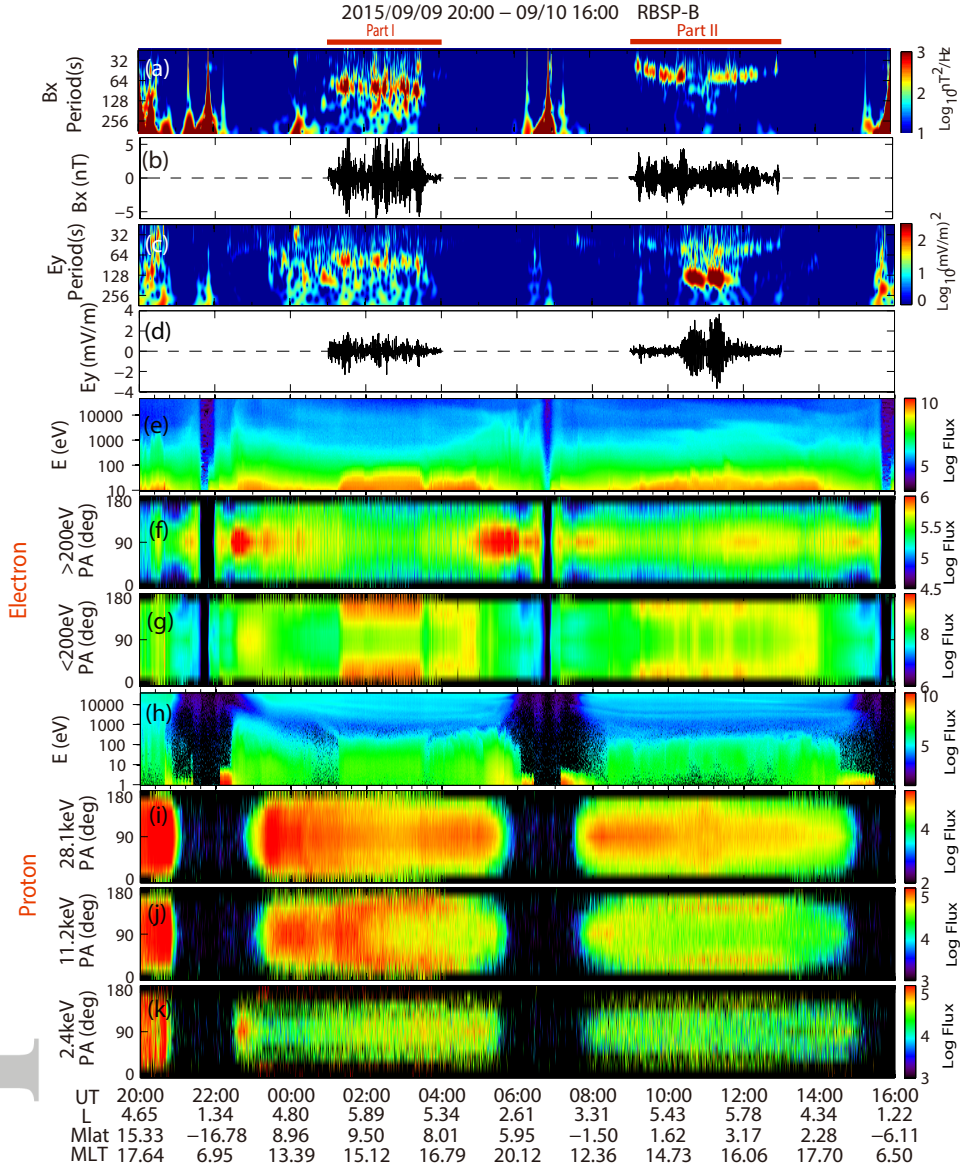

Figure 2. Overview of Van Allen Probe B observations: (a) Wavelet power spectrum of original B_x; (b) B_x component in GSE coordinates after subtracting the 10 min running average; (c) Wavelet power spectrum of original E_y; (d) E_y component after subtracting the 10 min running average; (e-g) Electron energy spectrum, pitch angle distributions with W>200 eV and W<200 eV, respectively; (h-k) Proton energy spectrum, pitch angle distributions in the energy channel of 28.1 keV, 11.2 keV and 2.4 keV, respectively. The red rectangular bars on the top illustrate the time intervals when there are distinct wave oscillations in two consecutive orbits. The L value, magnetic latitude (Mlat), and magnetic local time (MLT) are labelled at the bottom.

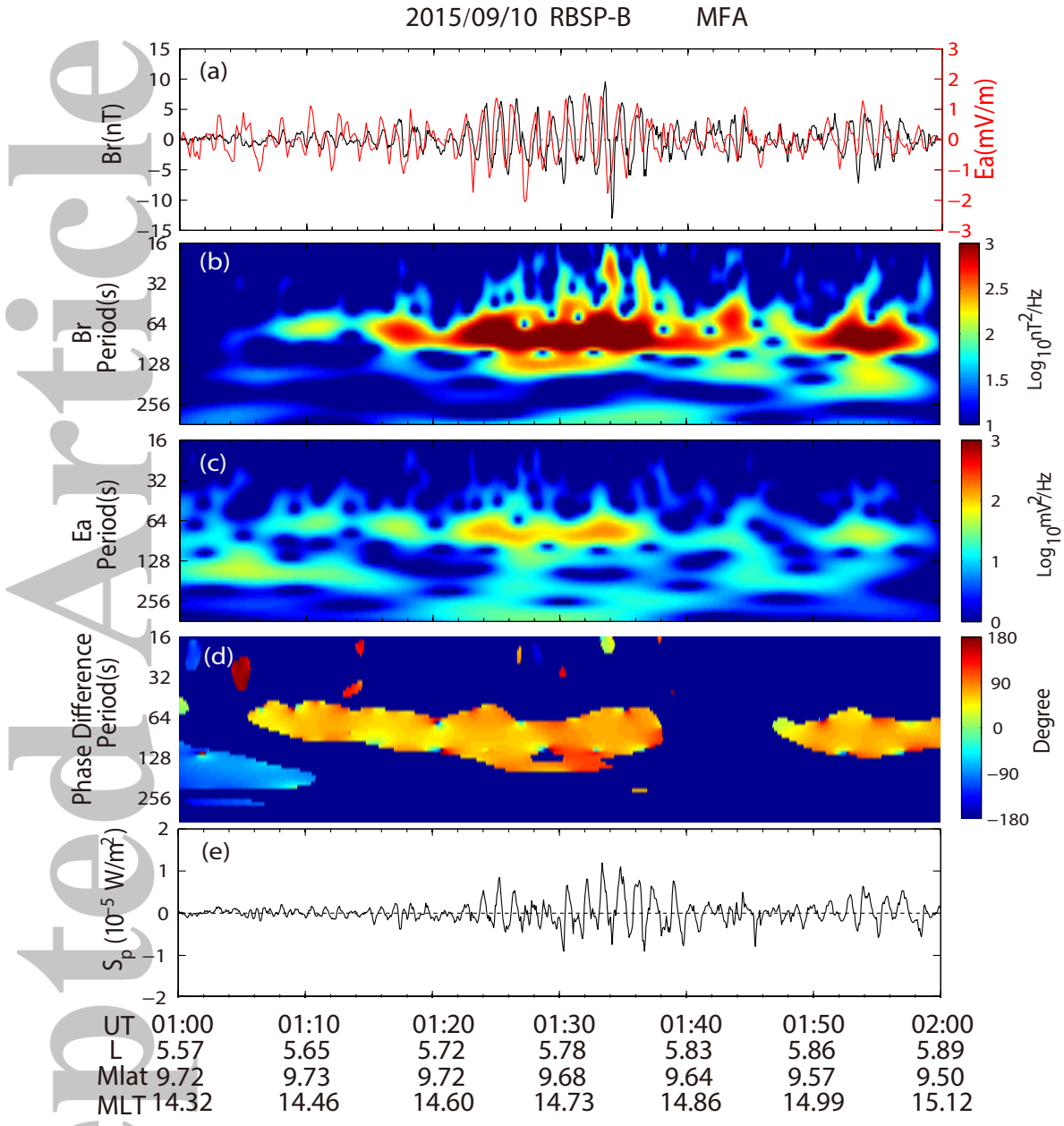

Figure 3. Properties of poloidal ULF waves. (a) Radial magnetic field component (B_r) indicated by black line and azimuthal electric field component (E_a) indicated by red line of poloidal ULF waves. (b-c) Wavelet power spectrum of B_r and E_a components, respectively. (d)Phase difference between E_a and B_r when coherence > 0.8. (e) Poynting vector in the parallel direction.

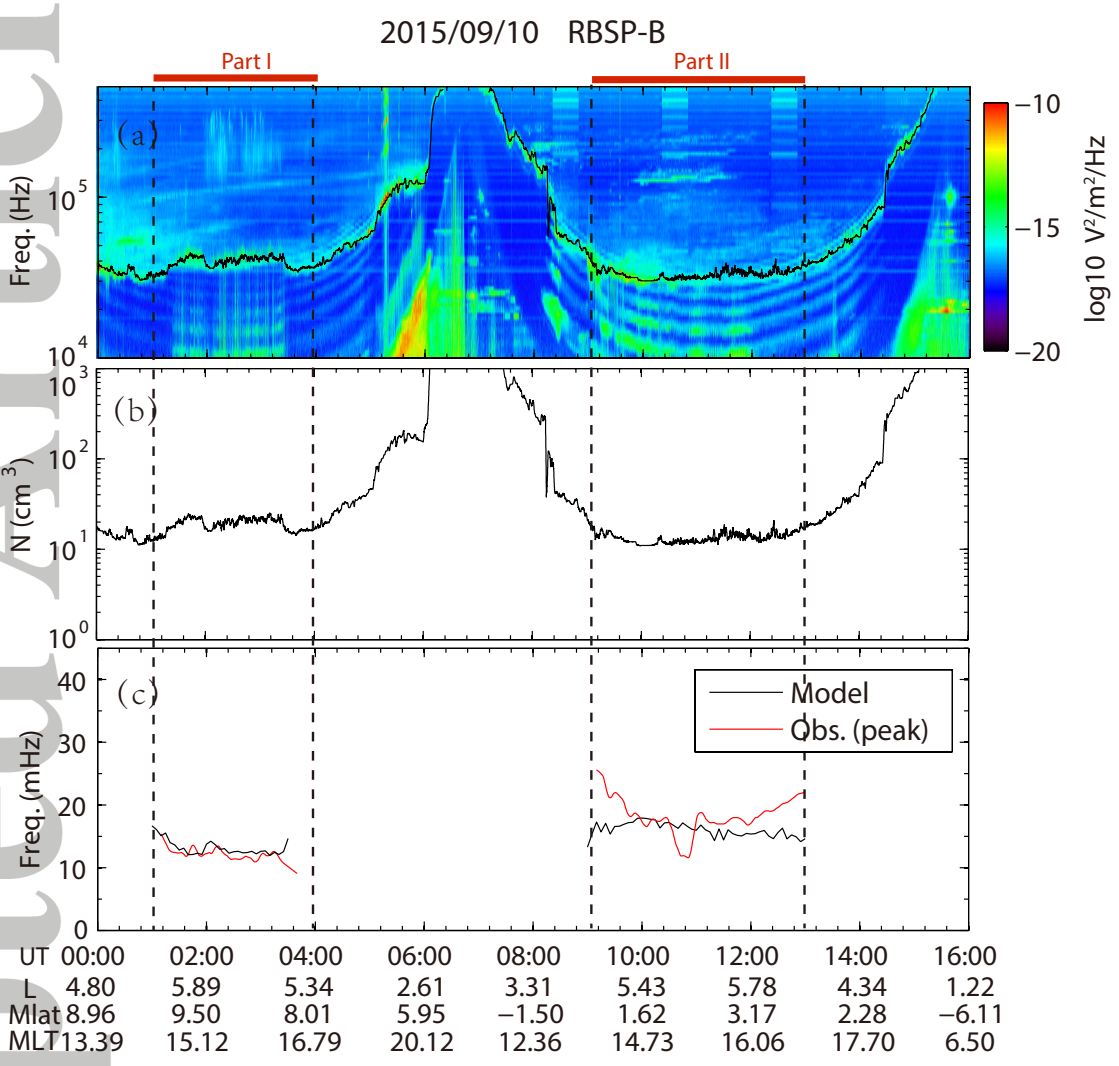

Figure 4. (a) Frequency-time spectrum of electric field spectral intensity from Probe B/EMFISIS. Black line represents the detected upper-hybrid resonance line. (b) The electron number density inferred from the detected upper-hybrid resonance line. (c) Eigenfrequency of second harmonic mode from modeling calculation (black), and peak frequency from wavelet power analysis of B_r component (red) during wave appearance.

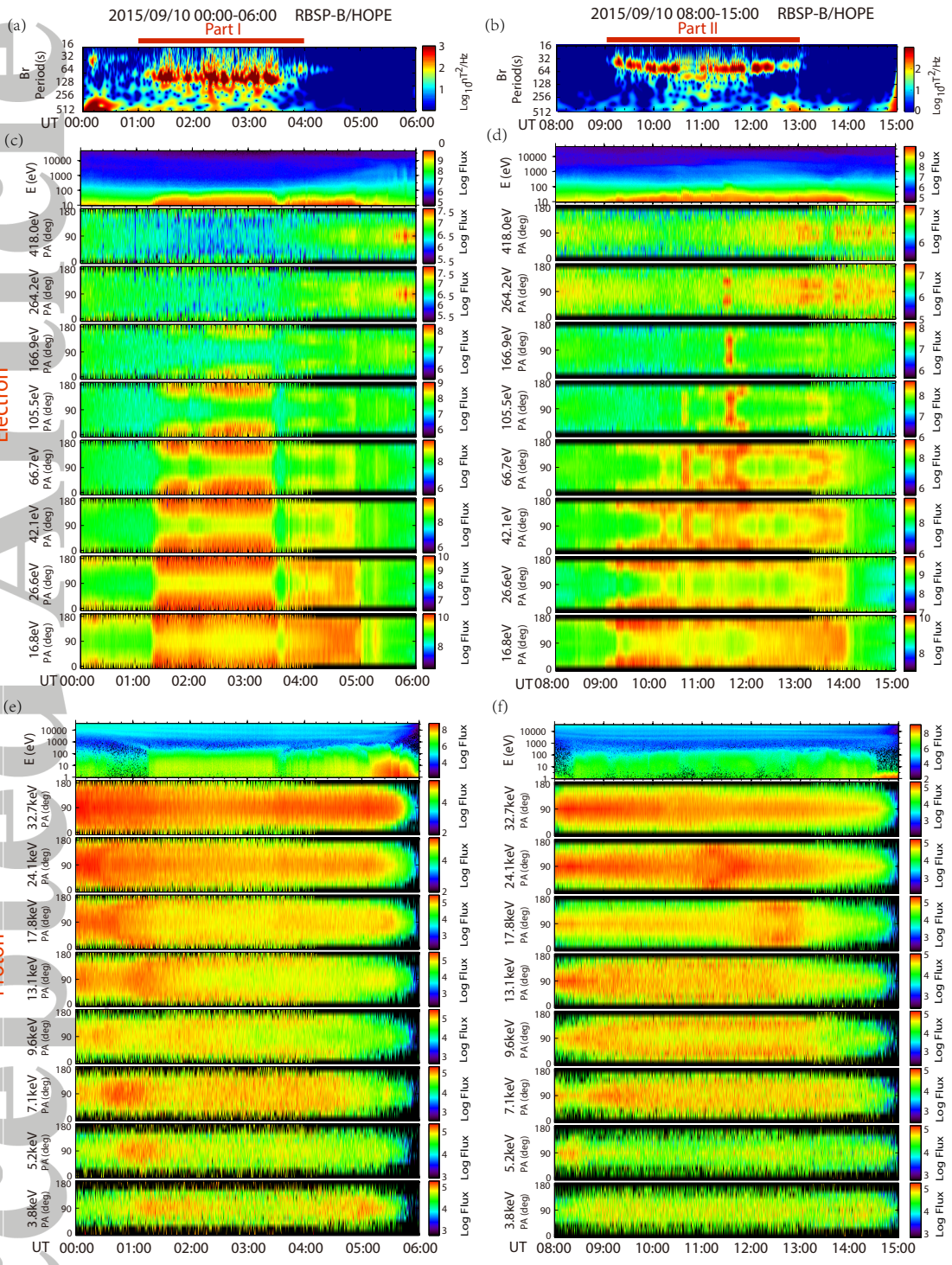

Figure 5. ULF wave, electron and proton observations from Van Allen Probe B during the time intervals of 00:00-06:00 and 08:00-15:00 on Sep. 10, 2015. (a and b) Wavelet power spectra of B_r component. (c and d) Energy spectra, pitch angle distributions in the energy range from 10 eV to 500 eV for electrons. (e and f) Energy spectra, pitch angle distributions in the energy range from 1 keV to 40 keV for protons.

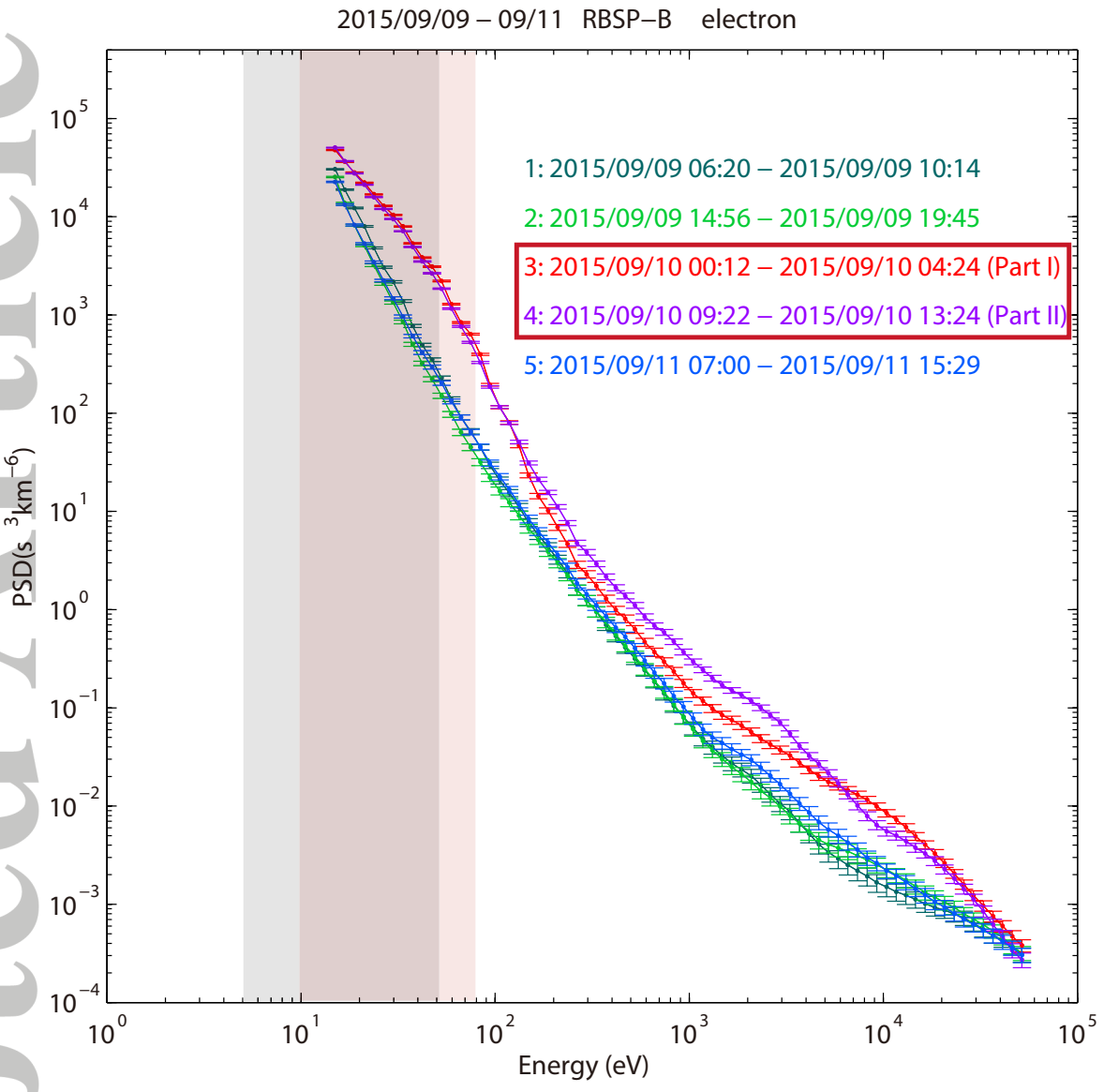

Figure 6. The averaged phase space density spectra of Probe B electrons with L>5 for two orbits before the ULF wave appearance (dark cyan and green), two orbits during the wave appearance (red and purple), and one orbit after the wave appearance (blue). The gray and red shadow regions indicate the resonant energy range corresponding to the B_r wave bandwidth, wavelet power dropping from maximum to its half value, in Part I and Part II, respectively.

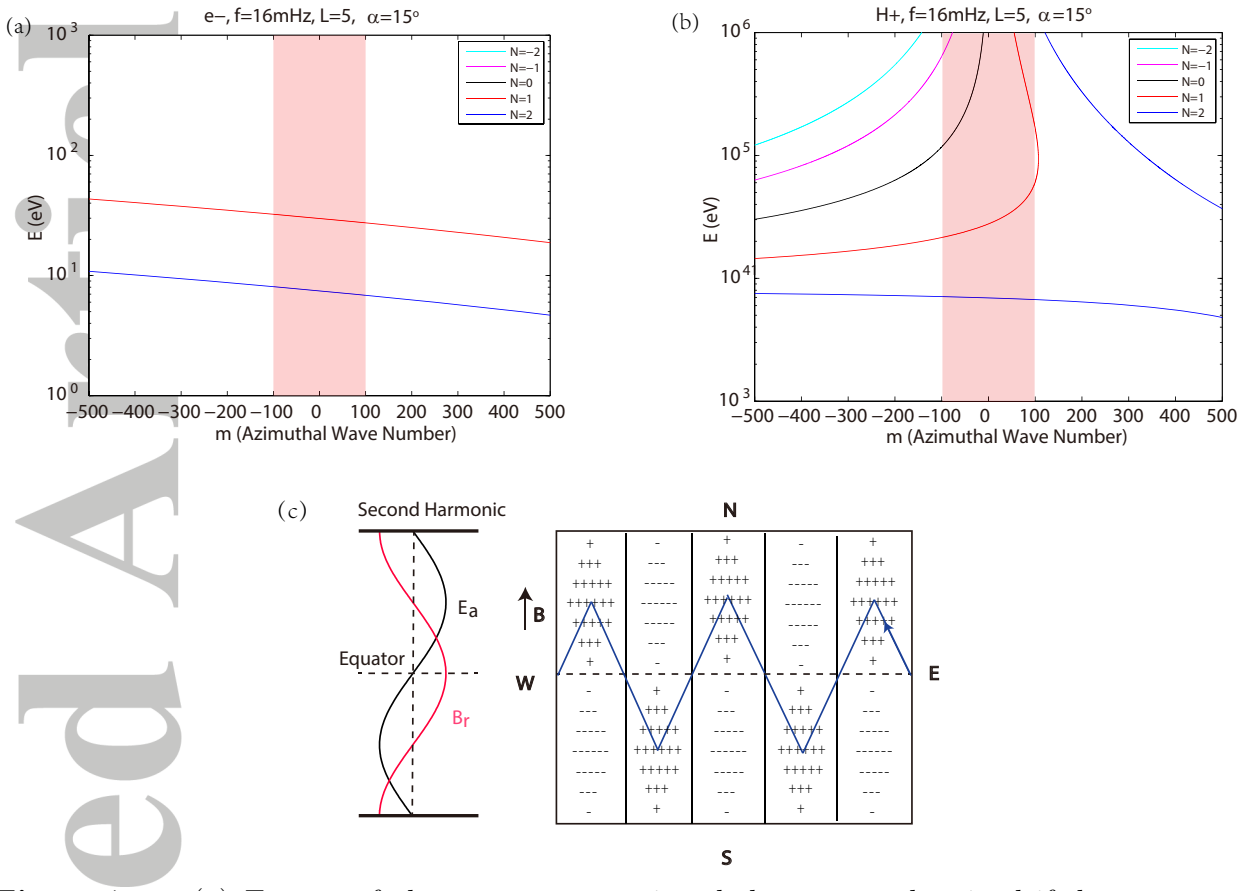

Figure 7. (a) Energy of electrons versus azimuthal wave number in drift-bounce resonant conditions with different N values. The wave frequency, L value, equatorial pitch angle are 16 mHz, 5 and 15 °; (b) The same as Figure 7a but for protons; (c) (left) Amplitude distributions of the second harmonic mode of electric field (black curve) and magnetic field (red curve) along the magnetic field line. (right) Schematic illustration of drift-bounce resonance with N=1 in the electric field wave frame of second harmonic mode. The blue line represents the guiding center trajectory of resonant particles. The plus and minus symbols indicate the westward and eastward electric fields, respectively.

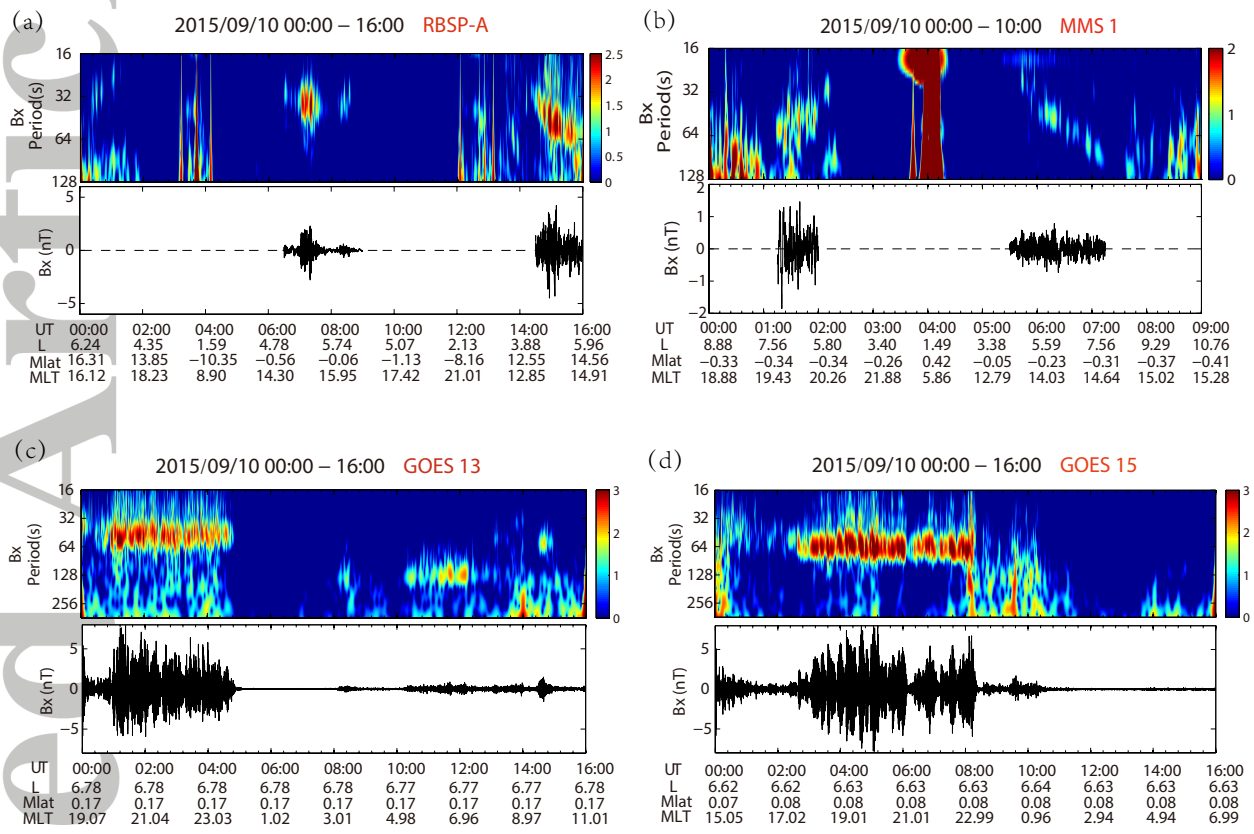

Figure 8. Wavelet power analysis of original B_x component in GSE coordinates and its oscillations after subtracting the 10 min running average for (a) Van Allen Probe A, (b) MMS 1, (c) GOES 13, and (d) GOES 15. The L value, magnetic latitude (Mlat), and magnetic local time (MLT) are labelled at the bottom.